International Journal of Electrical and Computer Engineering (IJECE)
Vol. 15, No. 5, October 2025, pp. 4395~4408
ISSN: 2088-8708, DOI: 10.11591/ijece.v15i5.pp4395-4408

Tomographic image reconstruction enhancement through median filtering and K-means clustering

Nguyen Quang Huy, Nguyen Truong Thang
Institute of Information Technology, Vietnam Academy of Science and Technology, Hanoi, Vietnam

Article Info

Article history:

Received Dec 3, 2024
Revised Jul 4, 2025
Accepted Jul 12, 2025

Keywords:

Distorted born iterative method
Image reconstruction
K-means clustering
Median filter
Ultrasound

ABSTRACT

Ultrasound tomography is a powerful and widely utilized imaging technique in the field of medical diagnostics. Its non-invasive nature and high sensitivity in detecting small objects make it an invaluable tool for healthcare professionals. However, a significant challenge associated with ultrasound tomography is that the reconstructed images often contain noise. This noise can severely compromise the accuracy and interpretability of the diagnostic information derived from these images. In this paper, we propose and rigorously evaluate the application of a median filter to address and mitigate noise artifacts in the reconstructed images obtained through the distorted born iterative method (DBIM). The primary aim is to enhance the quality of these images and thereby improve diagnostic reliability. The effectiveness of our proposed noise reduction approach is quantitatively assessed using the normalized error evaluation metric, which provides a precise measure of improvement in image quality. Furthermore, to enhance the interpretability and utility of the reconstructed images, we incorporate a basic machine learning technique known as K-means clustering. This method is employed to automatically segment the reconstructed images into distinct regions that represent objects, background, and noise. Hence, it facilitates a clearer delineation of different components within the images. Our results demonstrate that K-means clustering, when applied to images processed with the proposed median filter method, effectively delineates these regions with a significant reduction of noise. This combination not only enhances image clarity but also ensures that critical diagnostic details are preserved and more easily interpreted by medical professionals. The substantial reduction in noise achieved through our approach underscores its potential for improving the accuracy and reliability of ultrasound tomography in medical diagnostics.

Corresponding Author:

Nguyen Quang Huy
Institute of Information Technology, Vietnam Academy of Science and Technology
18 Hoang Quoc Viet, Cau Giay District, Hanoi, Vietnam
Email: quanghuy7889@gmail.com

1. INTRODUCTION

According to alarming statistics from the World Health Organization (WHO), approximately 10 million women worldwide succumb to breast cancer each year. This staggering figure underscores the critical importance of early detection in the battle against this pervasive disease. Early detection is not just beneficial but can be life-saving, as it significantly enhances survival rates—potentially increasing them by up to 25% [1]. Therefore, identifying abnormal tumors while they are still in their early stages is absolutely crucial. Mammography [2] is a widely employed screening tool for breast cancer, particularly among

postmenopausal women. However, its effectiveness is notably reduced in women under the age of 50. This age group typically has denser breast tissue, which poses a significant challenge for mammography. The dense tissue provides less contrast, making it difficult to detect small tumors. As a result, many cases may be missed, delaying critical treatment. In contrast, ultrasound technology presents a highly promising alternative for breast cancer diagnosis in younger women. Unlike mammography, ultrasound can penetrate dense breast tissue and visualize small tumors that might otherwise remain undetected. This makes it a valuable tool for early diagnosis and intervention in women who are under 50. The ability of ultrasound to effectively identify these small tumors could lead to earlier and more accurate diagnoses, ultimately improving survival rates and outcomes for this demographic [3]. Thus, integrating ultrasound into routine screening protocols for younger women could be a game-changer in the fight against breast cancer, potentially saving countless lives each year.

Ultrasound with frequencies ranging from 1 to 20 MHz [4] is one of the most widely used paradigms in biomedical imaging due to its safety, noninvasiveness, and non-ionizing nature, making it an invaluable tool for clinical diagnosis. This imaging modality has gained extensive application in medical settings, being utilized for a wide range of purposes, from obstetrics to cardiology and beyond. Despite its widespread use, conventional ultrasound machines rely on reflected signals, which present a significant limitation: they cannot accurately reproduce structures smaller than the wavelength of the ultrasound waves. In contrast, the ultrasound tomographic method offers a superior imaging approach with numerous advantages over traditional techniques such as X-ray [5], computed tomography (CT) [6], and magnetic resonance imaging (MRI) [7]. Ultrasound tomography operates on the principle of backscatter, enabling it to resolve structures smaller than the wavelength of the incident wave. This capability sets it apart from traditional imaging methods, which primarily rely on echo techniques. By leveraging material properties such as sound contrast, attenuation, and density, ultrasound tomography can effectively identify and visualize small-sized objects within the body. These advanced imaging capabilities not only enhance the accuracy of diagnoses but also expand the potential applications of ultrasound in medical practice. For instance, the improved resolution and contrast can aid in early detection of tumors, detailed imaging of soft tissues, and precise assessment of blood flow. Consequently, ultrasound tomography represents a significant advancement in medical imaging, offering a combination of safety, efficiency, and detailed resolution that is unmatched by many other imaging technologies.

Ultrasound tomography typically employs the Born approximation, which assumes that the scattering field is significantly smaller compared to the incident field. This approximation is widely accepted and has become a foundational concept in the field. In the realm of diffraction tomography, the distorted born iterative method (DBIM) is particularly popular due to its effectiveness in handling complex scattering problems [8]–[10]. Currently, the main application of this technique is only for breast imaging in women to detect cancer-causing cells [11]–[13]. However, the imaging process is often plagued by inherent noise, which can compromise the efficacy and clarity of DBIM-reconstructed images. To address this issue, we introduce a median filtering technique aimed at reducing noise without compromising the structural integrity of the images. Our study involves several key steps: the acquisition of ultrasound tomographic data, the reconstruction of these data using the DBIM method, and the subsequent application of the median filter to the reconstructed images. We meticulously analyze the impact of the median filter on noise reduction and overall image quality. To quantitatively assess the effectiveness of our approach, we employ evaluation metrics such as normalized error, which provides a robust measure of noise reduction efficacy. Moreover, various solutions leveraging machine learning algorithms have been proposed to enhance the quality of ultrasound images [14]–[18]. These approaches often involve complex computational techniques to improve image clarity and diagnostic accuracy. By integrating median filtering with DBIM and exploring machine learning enhancements, our study aims to provide a comprehensive solution to the challenges posed by noise in ultrasound tomography. The results demonstrate that our proposed method significantly reduces noise while maintaining the essential structural details of the images, thus improving the overall quality and reliability of ultrasound tomographic imaging.

In addition to devising an image restoration algorithm in DBIM utilizing the median filter, this study also advocates for the utilization of a machine learning algorithm to segment the reconstructed image into distinct domains of object, background, and noise. Image segmentation is a critical task in image processing, and while there are several sophisticated algorithms available for this purpose—such as mean-shift, the watershed algorithm, graph cut, region growing, the active contour model, convolutional neural networks (CNN), U-Net, and fuzzy C-means clustering—the simplicity and computational efficiency of K-means clustering make it the preferred choice for this study. Each of these advanced algorithms has its own strengths and applications; however, their complexity often demands significant computational resources and expertise, which may not be necessary for the segmentation needs in this context. Thus, a straightforward machine learning approach, K-means clustering, is employed to automatically divide the reconstructed image

into distinct domains representing objects, background, and noise. K-means clustering operates by partitioning the image data into clusters based on pixel intensity values, ensuring that pixels within the same cluster are more similar to each other than to those in different clusters. This method is not only efficient but also highly effective for the purpose of this study. The results demonstrate that K-means clustering effectively discriminates the regions in images obtained via the proposed method, significantly reducing the presence of noise in the recovered images. This enhancement in image quality underscores the potential of combining median filtering with K-means clustering for improved image segmentation and restoration in ultrasound tomography.

While the DBIM is a powerful inversion framework for ultrasound tomography, it is highly sensitive to noise in the measured data, often producing artifacts that obscure structural boundaries. Current methods either apply post-processing filters after reconstruction or rely on computationally intensive deep learning models, both of which pose limitations in real-time or resource-constrained applications. This study addresses that gap by embedding a computationally efficient median filtering step within each iteration of DBIM, thereby reducing noise accumulation early in the reconstruction process. Additionally, we introduce K-means clustering as a post-reconstruction segmentation tool to delineate meaningful regions in the image without requiring annotated training data. Together, these enhancements form a lightweight yet effective framework for improving image quality in practical ultrasound tomographic systems.

The remainder of this paper is organized as follows. Section 2 presents the theoretical foundation of ultrasound tomography, describes the DBIM, and introduces the proposed enhancement framework integrating median filtering and K-means clustering. Section 3 provides the simulation setup, evaluation metrics, and experimental results comparing the proposed method with conventional DBIM and dual-frequency DBIM. Section 4 discusses the key findings, compares with related work, addresses limitations, and outlines directions for future research. Finally, section 5 concludes the paper.

2. METHOD

The transceiver configuration diagram illustrates the setup of the ultrasound tomography system utilized in the DBIM, depicted in Figure 1. This diagram delineates the arrangement of transmitters and receivers within the system. The object under investigation is a minute cylindrical entity positioned within an expansive and uniform medium (in this case, a water environment). Our primary aim is to create a comprehensive image of this cylindrical object, designated as the region of interest (ROI). This ROI is meticulously partitioned into $N \times N$ squares, with each square representing a pixel, all sized uniformly at h. The configuration includes N_t transmitters and N_r receivers. The crux of our analysis lies in the objective function $Q(r)$, which is determined by (1):

$$\mathrm{Q}(\vec{r}) = \begin{cases} (2\pi f)^2 \left(\frac{1}{s_1^2} - \frac{1}{s_0^2}\right) \; if \; \vec{r} \le a \\ 0 \; if \;\; \vec{r} > a \end{cases} \tag{1}$$

where s_1 represents the speed of wave propagation through the object, while s_0 stands for the speed of propagation in the water medium. Meanwhile, the variable f denotes the ultrasonic wave frequency and a signifies the radius of the object.

Let's imagine an expansive realm characterized by a uniform medium, such as an endless expanse of water with a given wave number represented as k_0. In this context, the governing equation for the propagation of waves within this system can be succinctly expressed as (2):

$$\nabla^2 p(\vec{r}) + k_0^2 p(\vec{r}) = -\emptyset^{inc}(\vec{r}) - \mathrm{Q}(\vec{r}) p(\vec{r}) \tag{2}$$

where $p(\vec{r})$ represents the aggregate sound pressure throughout the given space, while $\emptyset^{\mathrm{inc}}(\vec{\mathrm{r}})$ signifies the sound source, with $\vec{\mathrm{r}}$ denoting the positional vector. The resolution of (2) becomes feasible through the utilization of Green's function $G_0(\vec{\mathrm{r}})$:

$$p^{sc}(\vec{r}) = p(\vec{r}) - p^{inc}(\vec{r}) = \int_{\Omega} \mathrm{Q}(\overrightarrow{r'}) p(\overrightarrow{r'}) G_0(\vec{r}, \overrightarrow{r'}) \, d\overrightarrow{r'} \tag{3}$$

where $p^{sc}(\vec{r})$ represents the scattering pressure, which signifies the pressure resulting from the scattering phenomenon. Conversely, $p^{inc}(\vec{r})$ denotes the incident wave pressure generated by the source $\emptyset^{\mathrm{inc}}(\vec{\mathrm{r}})$. The parameter Ω pertains to the spatial extent of the object intended for imaging.

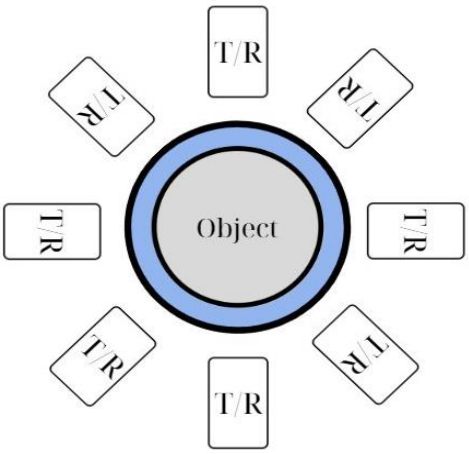

Figure 1. Transceiver configuration diagram

Given the assumption of a uniform environment surrounding the object, the Green function is found to be proportional to the zero-order Hankel function, denoted as $H_0^{(2)}(k_0 r)$ or $e^{(-ik_0 r)/r}$, extending to both two-dimensional and three-dimensional spaces. Equation (3) delineates the forward problem equation, serving the purpose of computing the pressure at any point outside Ω, once the aggregate pressure for all $\vec{r}$ within Ω has been determined.

$$0(\vec{r} = k(\vec{r})^2 - k_0^2$$

Equation (3) lends itself to discretization through the method of moments (MoM) [8], wherein it can be represented in matrix form. This process involves transforming the continuous equations into a discrete form suitable for computational analysis. By discretizing (3) using MoM, we derive a matrix equation governing the calculation of sound pressure within the region of interest (ROI):

$$\bar{p} = \left(\bar{I} - \bar{V}.D(\bar{Q})\right)p^{inc} \tag{4}$$

The calculation of scattering pressure outside the ROI area is performed as (5):

$$\bar{p}^{sc} = \bar{U}.D(\bar{Q}).\bar{p} \tag{5}$$

where $\bar{I}$ represents the identity matrix, and $D(\bullet)$ denotes the diagonalization operator, $\bar{U}$ emerges as the matrix embodying coefficients pertinent to the Green function $G_0(r, r')$ originating from each pixel point towards the receiver. Conversely, $\bar{V}$ embodies coefficients associated with the Green function $G_0(r, r')$ delineating interactions between pixels. Both $\bar{U}$ and $\bar{V}$ matrices undergo calculation as (6):

$$G(\vec{r}, \vec{r}_{m\,n}) = \int G_0\left(\vec{r}, \overrightarrow{r'}\right) b_{mn}(\overrightarrow{r'})\, d\overrightarrow{r'} \tag{6}$$

here, $b_{mn}(\overrightarrow{r'})$ represents the basic sinc function. In the inverse problem, our objective is to determine $Q(\vec{r})$ given a set of measurements of the sound field $p(\vec{r}, k)$ within the scattering region. However, if the wave number $k(\vec{r})$ is unknown, then (3) cannot be directly utilized to compute the object function because $p(\vec{r}, k)$, where $\vec{r} \in \Omega$, is also unknown. Introducing the function $k(\vec{r})$ into consideration, Equation (3) can be reformulated as (7):

$$p(\overrightarrow{r}, k) = p^{inc,k_r}(\vec{r}) + \int_\Omega \Delta Q(\overrightarrow{r'}) p(\overrightarrow{r'}, k) G_r\left(\vec{r}, \overrightarrow{r'}\right) d\overrightarrow{r'} \tag{7}$$

within this context, the symbol $p(\overrightarrow{r'}, k)$ denotes the sound pressure corresponding to the wave number function $k(\vec{r})$, $p^{inc,k_r}(\vec{r})$ represents the sound pressure up to the background wave number $k_r(\vec{r})$ and

$$\Delta Q(\vec{r}) = Q(\vec{r}) - Q_r(\vec{r}) \tag{8}$$

$$\mathrm{Q}_r(\vec{r}) = \mathrm{k}_\mathrm{r}^2(\vec{r}) - \mathrm{k}_0^2 \tag{9}$$

In order to transform the inverse problem into a linear form that incorporates the unknown function $k(\vec{r})$, we employ the first-order Born approximation method, wherein $\mathcal{p}(\vec{r},k) \approx \mathcal{p}^{inc,k_r}(\vec{r}) = \mathcal{p}(\vec{r},k_r)$. This approximation facilitates the simplification of the complex relationship between the measured data and the unknown function $k(\vec{r})$, enabling a more tractable solution to be obtained. By adopting this method, we effectively linearize the problem as (10):

$$\mathcal{p}(\vec{r},k) - \mathcal{p}(\vec{r},k_r) \approx \int \Delta\mathrm{Q}(\vec{r'})\mathcal{p}(\vec{r'},k_r)G_r\left(\vec{r},\vec{r'}\right)d\vec{r'} \tag{10}$$

Equation (10) serves as the foundational inverse problem equation. When a specific value for $k_r(\vec{r})$ is selected, it enables the computation of $\mathcal{p}(\vec{r},k_r)$ and $G_r\left(\vec{r},\vec{r'}\right)$ utilizing the forward problem approach. Central to (10) lies the unknown variable $k(\vec{r})$, which encapsulates vital information. Moreover, (10) holds the potential for discretization through the method of moments (MoM) as (11), (12):

$$\Delta\bar{\mathcal{p}}^{sc} = \bar{M}.\Delta\overline{\mathrm{Q}} \tag{11}$$

$$\overline{\mathrm{M}} = \overline{\mathrm{U}}.\mathrm{D}(\bar{\mathcal{p}}) \tag{12}$$

In this context, $\Delta\bar{\mathcal{p}}^{sc}$ represents the difference between two vectors, where $\bar{\mathcal{p}}^{sc}$ denotes the vector containing the values of the predicted scattering field $\mathcal{p}(\vec{r},k_r)$, and $\bar{\mathcal{p}}^{sc,m}$ denotes the vector containing the values of the measured scattering field $\mathcal{p}(\vec{r},k)$. Essentially, $\Delta\bar{\mathcal{p}}^{sc}$ quantifies the deviation between the predicted and measured scattering fields. Additionally, $\Delta\overline{\mathrm{Q}}$ stands for another vector comprising the values of $\Delta\mathrm{Q}(\vec{r})$.

Noted that the unknown vector $\overline{\mathrm{Q}}$ consists of $N\times N$ variables, which corresponds to the number of pixels within the ROI. The process of estimating the object function involves iterative procedures that iteratively update the elements of $\overline{\mathrm{Q}}$ to converge towards the optimal solution. These iterative processes are essential for accurately reconstructing the object function from the ultrasound tomography data, as they refine the estimation of pixel values within the ROI, enhancing the overall quality of the reconstructed image.

$$\overline{\mathrm{Q}}^{\mathrm{n}} = \overline{\mathrm{Q}}^{(\mathrm{n}-1)} + \Delta\overline{\mathrm{Q}}^{(\mathrm{n}-1)}, \tag{13}$$

at the current step, $\overline{\mathrm{Q}}^{n}$ and $\overline{\mathrm{Q}}^{(n-1)}$ denote the object functions representing the present and previous states, respectively. To quantify the variation between these states, we compute $\overline{\mathrm{Q}}$, signifying the change in $\overline{\mathrm{Q}}$, which can be determined by addressing the l_2 nonlinear regularization problem. This problem aims to optimize the regularization parameter to minimize the discrepancy between $\overline{\mathrm{Q}}^{n}$ and $\overline{\mathrm{Q}}^{(n-1)}$, thereby providing insight into the evolution of the object functions across iterations. Consequently, this approach facilitates a comprehensive understanding of the iterative process, enhancing the effectiveness of the optimization scheme in achieving convergence towards an optimal solution.

$$\Delta\overline{\mathrm{Q}} = \arg\min_{\Delta\overline{\mathrm{Q}}}\left\|\Delta\bar{\mathcal{p}}^{\mathrm{sc}}{}_{\mathrm{t}} - \overline{\mathrm{M}_{\mathrm{t}}}\Delta\overline{\mathrm{Q}}\right\|_2^2 + \epsilon\|\Delta\overline{\mathrm{Q}}\|_2^2, \tag{14}$$

here, $\Delta\bar{\mathcal{p}}^{sc}$ represents a vector of dimensions $N_tN_r \times 1$, encapsulating the disparities between the anticipated and actual scattered ultrasound signals. Concurrently, $\bar{M}_t$ denotes the system matrix with dimensions $N_tN_r \times N^2$. Lastly, ϵ serves as the regularization parameter, influencing the regularization process within the system. This parameter plays a crucial role in balancing the trade-off between fitting the observed data and controlling the complexity of the solution. Adjusting ϵ allows for the fine-tuning of the reconstruction process, ensuring optimal results tailored to the specific characteristics of the ultrasound tomography system under consideration. Therefore, understanding and appropriately selecting the value of ϵ are fundamental steps in achieving accurate and reliable reconstructions.

In the context of a two-dimensional scenario, the incident pressure corresponding to a zero-order Bessel beam can be succinctly expressed as (15):

$$\overline{\mathcal{p}}^{\mathrm{inc}} = \mathrm{J}_0(\mathrm{k}_0|\mathrm{r}-\mathrm{r}_\mathrm{k}|), \tag{15}$$

here, J_0 refers to the zeroth-order Bessel function, the term $|r - r_k|$ denotes the Euclidean distance between the transmitter and the k^{th} point within the ROI.

The median filter is widely utilized in image processing due to its numerous advantages, particularly in the realms of noise reduction and image feature preservation. When it comes to noise reduction, the median filter stands out for its efficacy in addressing various types of noise present in images, such as salt-and-pepper noise and impulse noise. By substituting pixel values with the median value derived from neighboring pixels, the filter effectively eliminates outliers and irregularities induced by noise, resulting in a more refined and cleaner image. In terms of preserving edges and intricate details, the median filter offers distinct advantages over mean filters, which tend to blur edges and fine features. Due to the inherent robustness of the median value to extreme values, the filter excels in retaining the structural integrity of the image while concurrently reducing noise, making it particularly suitable for applications where edge preservation is paramount. Furthermore, the median filter boasts a straightforward implementation process, rendering it relatively easy to deploy and computationally efficient. This simplicity renders it a favored option for real-time image processing tasks, especially when confronted with filter windows of moderate size. Consequently, the versatility and efficiency of the median filter make it an indispensable tool in various image processing applications, contributing significantly to enhancing image quality and extracting pertinent information.

Algorithm 1 outlines the procedure for the filtered distorted born iterative method (Filtered DBIM). This method incorporates a series of steps to effectively address noise artifacts in the reconstructed images. Initially, the algorithm begins by acquiring the noisy input image by using the DBIM. Subsequently, it applies a median filter to the input image to reduce the noise present. Following the noise reduction step, the filtered image undergoes reconstruction using the DBIM, which aims to produce a clearer representation of the underlying structure. Throughout this process, the algorithm iteratively refines the reconstructed image until a satisfactory level of accuracy is achieved. By integrating the median filtering technique into the DBIM framework, the algorithm enhances the quality of the reconstructed images, thus improving the overall effectiveness of the ultrasound tomography imaging system.

Algorithm 1. The Filtered DBIM

Set up the transceiver configuration for imaging system
Opt initial values: $\bar{Q}_{(n)}= \bar{Q}_{(0)}$ and $\bar{\chi}_0 = \bar{\chi}^{inc}$ by (15)
For $n = 1$ *to* N_{sum}, **do**
1. Determine $\bar{U}$ and $\bar{V}$
2. Determine $\chi, \bar{\chi}^{sc}$ corresponding to $\bar{Q}_{(n)}$ by (4, 5)
3. Determine $\Delta\bar{\chi}^{sc}$ by (11)
4. Determine $\Delta\bar{Q}_{(n)}$ by (14)
5. Determine $\bar{Q}_{(n+1)} = \bar{Q}_{(n)} + \Delta\bar{Q}_{(n)}$
6. Remove noise for $\bar{Q}_{(n+1)}$ by median filter.
End For

The resulting image encompasses areas representing the object, background, and noise, providing crucial insights into the underlying structure of the data. Thus, the continued utilization of the K-means clustering method aims to delineate these regions automatically, facilitating the identification of anomalous objects and the observation of regions heavily affected by noise. K-means clustering stands as a widely employed algorithm for image segmentation, tasked with partitioning an image into distinct segments or regions, thereby aiding in the extraction of meaningful information. This algorithm allocates each pixel to one of K clusters based on its intensity values, effectively grouping together pixels with similar characteristics. In our simulation scenario, we opt for a cluster count (K) of three, aligning with the three specific regions of interest: the area containing the object, the background area, and the noise-affected area. This deliberate choice enables a focused analysis of each region, allowing for a more nuanced understanding of the underlying data distribution and enhancing the accuracy of subsequent processing steps.

To clarify the contributions, we summarize the proposed method as follows. The core innovation lies in integrating a 2D median filter directly into the iterative reconstruction loop of DBIM. After each DBIM iteration, the reconstructed object function is denoised using a median filter to suppress localized noise without blurring critical structural edges. This intra-loop filtering reduces error accumulation and improves convergence stability. Once the final image is obtained, we apply K-means clustering (with K=3) to segment the image into distinct zones: the object (target), the homogeneous background, and residual noise. This post-processing step is designed to enhance the interpretability of the reconstruction and to isolate relevant diagnostic features. The algorithmic workflow is outlined in Algorithm 1 and validated in Section 3.

3. SIMULATIONS AND RESULTS

The simulation parameters for this study encompass various facets essential for the accurate depiction of ultrasound tomography. Specifically, the incident frequency f is set at 1 MHz in order to satisfy

the Born approximation condition. To ensure comprehensive coverage, both the number of transmitters (N_t) and the number of receivers (N_r), collectively defining the number of measurements ($N_t \times N_r$), are meticulously calibrated. Moreover, to achieve robust convergence and precise reconstruction, a total of N_{sum}=5 iterations are iteratively executed. The spatial resolution within the region of interest is finely partitioned into N=12 pixels per axis, thereby yielding N^2=144 variables in two-dimensional space. Additionally, the scattering area diameter, spanning 10 mm, and the sound contrast set at 10% are tailored. Finally, the distances from both transmitters and receivers to the center of the object are defined at 60 mm.

To simulate realistic conditions, we incorporated additive Gaussian noise into the measured scattered field data. Specifically, we added zero-mean Gaussian noise with a standard deviation corresponding to 5% of the maximum amplitude of the measured signal. This choice reflects the typical noise encountered in practical ultrasound systems, including electronic noise, amplifier-induced variations, and environmental disturbances during wave propagation.

Figure 2 depicts the ideal inverse-scattering pattern requiring reconstruction. Figure 3 illustrates the normalized error observed after N_{sum} iterations of both the conventional DBIM and the filtered DBIM for N_t=N_r=6. It is evident from the overall trend that the filtered DBIM consistently surpasses the conventional DBIM in terms of reducing normalized error. This trend underscores the significant contribution of the filtering process within the DBIM framework towards enhancing accuracy and facilitating convergence across multiple iterations. Notably, when comparing the two approaches, the filtered DBIM exhibits reduced percentages in normalized error from the initial iteration to the fifth iteration, amounting to 6.84%, 36.73%, 51.95%, 58.52%, and 62.78%, respectively. These reduced percentages serve as quantitative indicators of the enhancement achieved by the filtered DBIM. Higher reduction percentages signify a more efficacious filtering process, leading to a considerable decrease in normalized error and consequently, enhanced accuracy. This discernible improvement in accuracy compared to the conventional DBIM highlights the efficacy of the filtering process throughout the iterations, a phenomenon further elucidated in Figure 4.

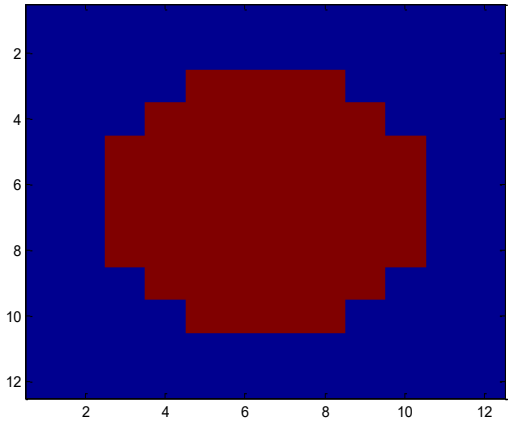

Figure 2. Ideal inverse scatter target

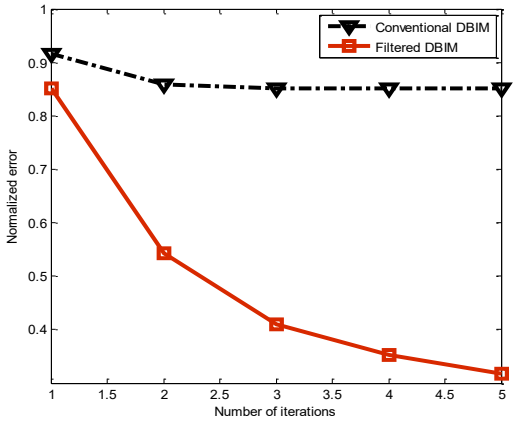

Figure 3. Normalized error after N_{sum} iterations of the conventional DBIM and filtered DBIM when N_t=N_r=6

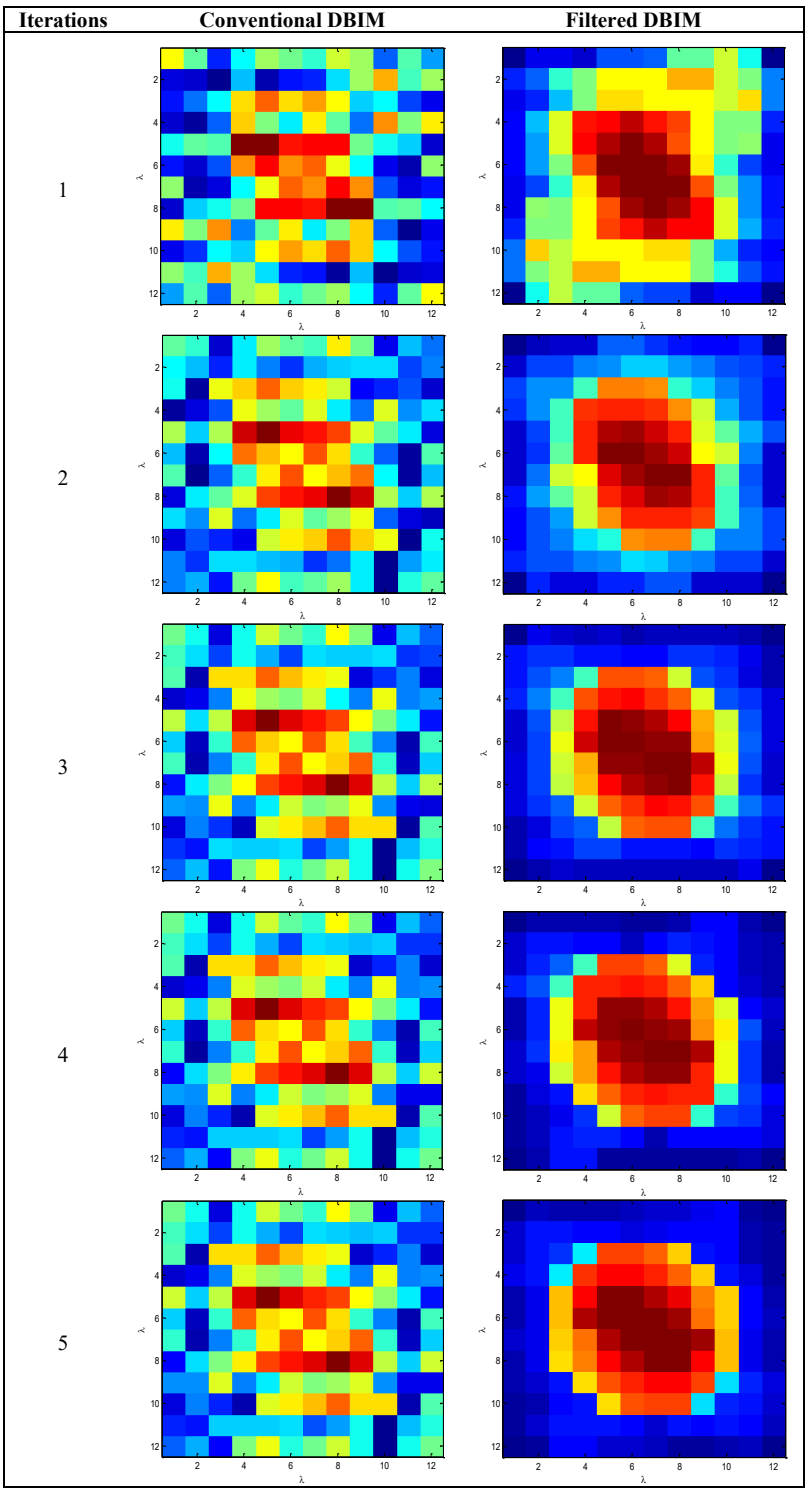

Figure 4. Recovered images after each iteration of the conventional DBIM and filtered DBIM when N_t=N_r=6

Figure 5 illustrates the evolution of normalized error over multiple iterations of both the conventional DBIM and the filtered DBIM methods with $N_t = N_r = 10$. Initially, during the first iteration, the filtered DBIM exhibits a modest yet discernible decrease in normalized error, amounting to approximately 0.97% compared to the conventional DBIM. As the iterations progress, the superiority of the filtered DBIM becomes increasingly evident. By the final iteration, it achieves a remarkable reduction of approximately 86.39% in normalized error compared to the conventional DBIM. This consistent outperformance is observed throughout all iterations, with reductions ranging from 0.97% to 86.39%. The

trend underscores a significant and escalating enhancement in performance as iterations advance, underscoring the efficacy of the filtering mechanism within the DBIM framework. Moreover, Figure 6 provides a visual representation indicating the convergence of the recovery function towards the ideal objective function after each iteration. This convergence suggests that the filtered DBIM method steadily approaches the desired outcome with each successive iteration, further affirming its efficacy and potential for practical application in ultrasound tomography.

Figure 7 illustrates the progression of normalized error throughout N_{sum} iterations for both the conventional DBIM and the filtered DBIM when N_t=N_r=12. In the initial iteration, the normalized errors for the conventional and filtered DBIM are recorded as 0.9697 and 0.9472, respectively. Conversely, in the final iteration, the normalized errors for the conventional and filtered DBIM decrease to 0.1711 and 0.0934, respectively. Notably, during the initial iteration, the discrepancy in normalized error between the two methods remains minimal, with the filtered DBIM exhibiting a slight advantage, showcasing a 2.32% reduction in normalized error compared to the conventional DBIM approach. However, as the iterations progress, the superiority of the filtered DBIM becomes more pronounced. By the final iteration, the filtered DBIM outperforms the conventional DBIM significantly, demonstrating a notable 45.40% reduction in normalized error. This consistent pattern of improved performance is observed across all iterations, with the disparity between the two methods becoming more evident towards the end of the process. For a comprehensive visualization of this trend, refer to Figure 8, which further elucidates the widening gap in performance between the conventional and filtered DBIM approaches.

Analysis reveals that Figures 3, 5, and 7 illustrate the normalized error following N_{sum} iterations for both the conventional DBIM and the filtered DBIM under different scenarios, specifically for N_t=N_r=6, N_t=N_r=10, and N_t=N_r=12, respectively. Notably, a significant decrease in normalized error is observed for the cases where N_t=N_r=6, N_t=N_r=10, indicating the considerable efficacy of the proposed method when the number of measurements is less than the number of variables. This observation aligns with practical scenarios in high-resolution imaging, where such conditions frequently occur due to various constraints. Consequently, the findings suggest the potential robustness and applicability of the proposed method across a range of practical settings in the field of imaging.

Figure 9 illustrates the comparison between the ideal, reconstructed, and segmented images obtained using both the conventional DBIM and the filtered DBIM methods for two scenarios: when N_t=N_r=6 and N_t=N_r=10 after N_{sum} iterations. In the segmentation process, three clusters (K) are utilized to represent distinct regions within the images: those containing objects, background areas, and noise. The outcomes indicate a notable difference between the two methods. The image reconstructed via the conventional DBIM approach exhibits substantial noise interference, with noise artifacts apparent within both the object and spread across the background. Conversely, the reconstructed image obtained through the filtered DBIM method displays minimal noise presence, showcasing the effectiveness of this technique in noise reduction. Furthermore, the resulting image from the filtered DBIM closely resembles the ideal image, underscoring the accurate separation of object and background regions achieved through K-means clustering. This starkly contrasts with the conventional DBIM method, where even after the final iteration, the decomposed object notably deviates from the ideal reference image. These findings emphasize the superior noise reduction capabilities and overall effectiveness of the filtered DBIM method in image reconstruction compared to its conventional counterpart.

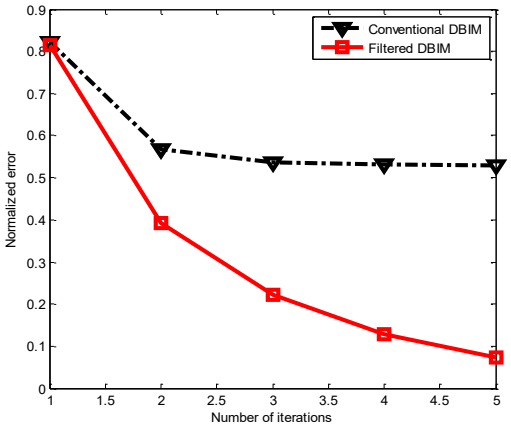

Figure 5. Normalized error after N_{sum} iterations of the conventional DBIM and filtered DBIM when $N_t = N_r = 10$

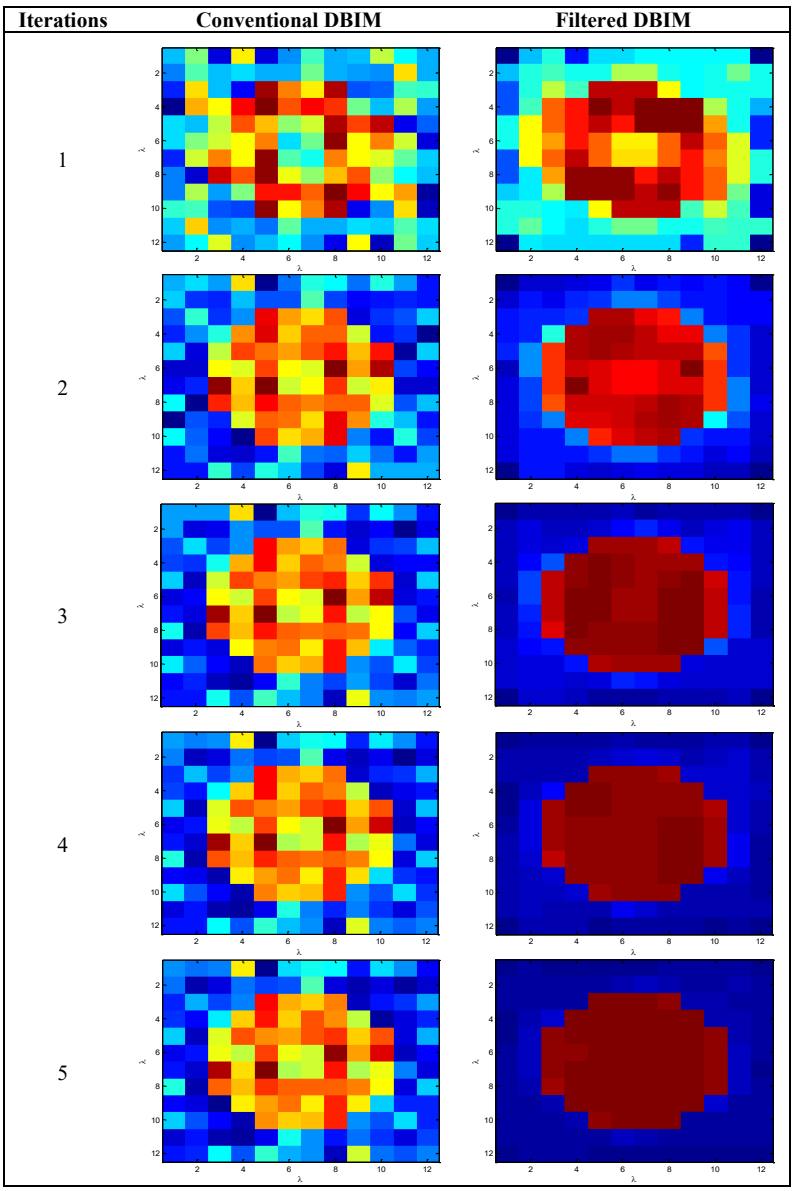

Figure 6. Recovered images after each iteration of the conventional DBIM and filtered DBIM when N_t=N_r=10

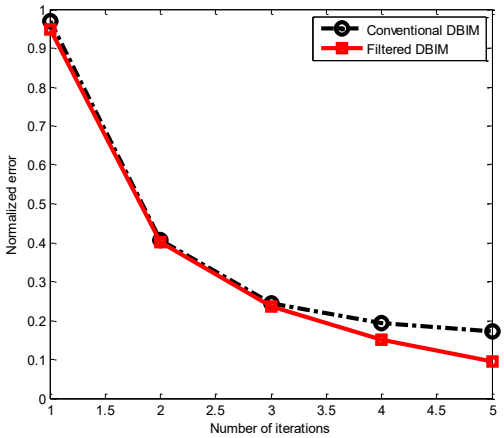

Figure 7. Normalized error after N_{sum} iterations of the conventional DBIM and filtered DBIM when N_t=N_r=12

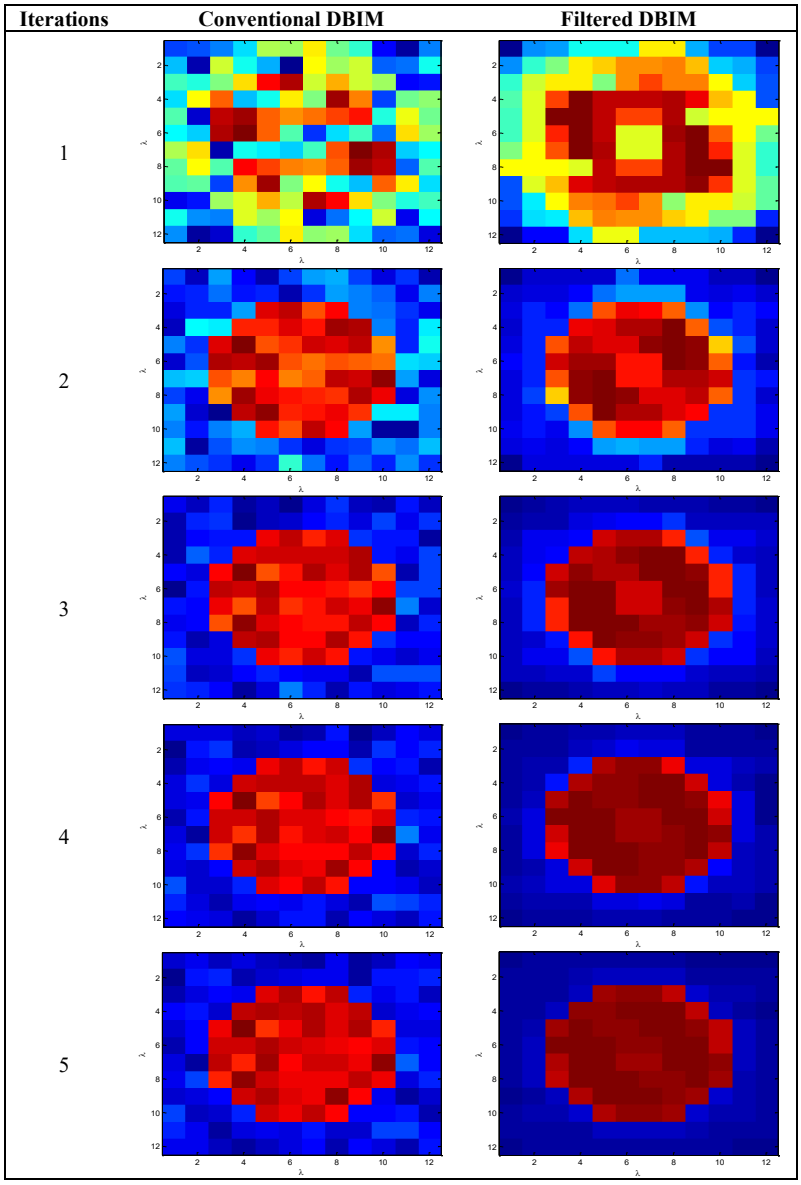

Figure 8. Recovered images after each iteration of the conventional DBIM and filtered DBIM when N_t=N_r=12

To illustrate the efficacy of the filtered DBIM method under conditions where the number of measurements is smaller than the number of variables, we conduct a comparative analysis of the normalized error between the filtered DBIM and dual-frequency DBIM (DF-DBIM) [19]–[22] techniques, as outlined in Table 1. The DF-DBIM methodology leverages two distinct frequencies, namely f_1 (low) and f_2 (high), to estimate sound contrast in N_{f1} and N_{f2} iterations correspondingly. This dual-frequency approach offers the inherent advantage of expediting convergence speed during the process of image restoration. Specifically, simulation parameters in DF-DBIM are defined as f_1=1 MHz, f_2=2 MHz, N_{f1}=2, N_{f2}=3, while keeping other parameters constant. As delineated in Table 1, the filtered DBIM method exhibits a notably superior convergence rate compared to the DF-DBIM method, as evidenced by the diminished normalized error observed at each iteration. Remarkably, right from the initial iteration, the filtered DBIM technique visibly showcases a superior convergence pace over DF-DBIM. This disparity underscores the enhanced performance of the filtered DBIM approach, particularly when dealing with a constrained number of measurements relative to variables.

It should be noted that the current study uses simulated ultrasound data generated under controlled conditions using a physical forward model and known ground-truth objects. While real clinical ultrasound images have not yet been evaluated in this work, the use of simulation allows for precise quantification of reconstruction errors and direct benchmarking against ideal targets. This provides a rigorous foundation for future application of the method to real-world datasets, which we plan to address in subsequent studies.

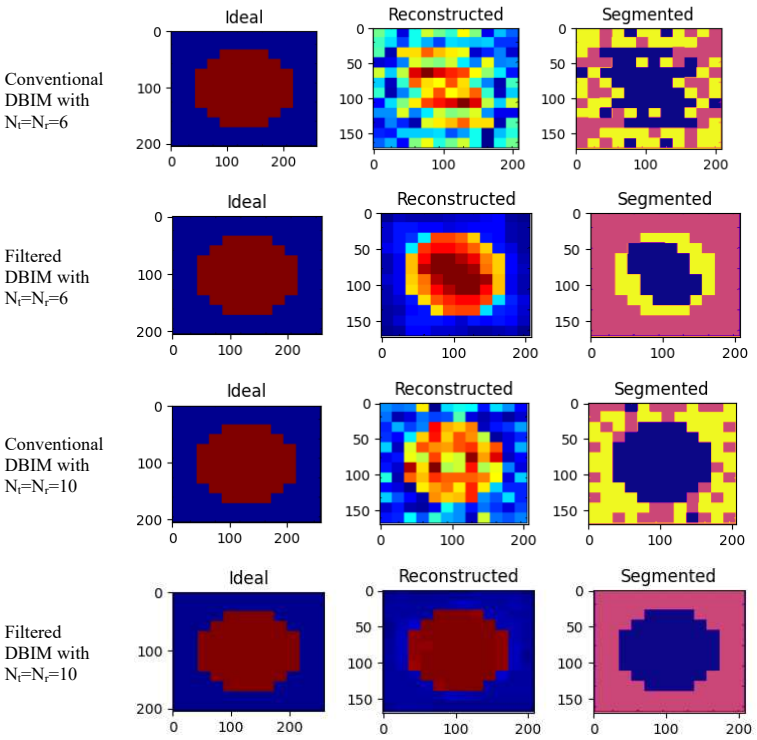

Figure 9. The ideal, recovered and segmented images by the conventional DBIM and the filtered DBIM after N_{sum} iterations

Table 1. Normalized error evaluation of the DF-DBIM and Filtered DBIM approaches

Scenarios	Methods	Normalized error after each iteration				
N_t=N_r=6	DF-DBIM	0.9157	0.8583	0.5153	0.5145	0.5200
	Filtered DBIM	0.8520	0.5433	0.4091	0.3526	0.3171
N_t=N_r=10	DF-DBIM	0.822	0.5684	0.2374	0.1818	0.1698
	Filtered DBIM	0.8144	0.3929	0.2223	0.1280	0.0721

4. DISCUSSION

This study introduces a filtered image reconstruction framework for ultrasound tomography by embedding median filtering within the iterative process of the DBIM, followed by post-reconstruction K-means clustering for segmentation. The simulation results consistently demonstrate that the proposed method significantly reduces normalized error in comparison with both conventional DBIM and dual-frequency DBIM (DF-DBIM) methods across different configurations. The enhanced reconstructions closely approximate the ideal object function, with sharper boundaries and less noise interference. Furthermore, the application of K-means clustering provides a clear delineation between object, background, and noise regions, thereby improving the interpretability of the reconstructed images.

Our approach distinguishes itself from prior works that either apply denoising as a post-processing step or rely on complex deep learning architectures for enhancement. Previous studies such as [19] and [22] leveraged dual-frequency strategies to improve convergence and contrast but remained susceptible to noise in low-measurement regimes. By integrating a denoising operation directly into the DBIM iterative loop, our method effectively suppresses the propagation of noise throughout the inversion process. Additionally, while machine learning-based segmentation methods like CNN or fuzzy C-means clustering have been proposed in literature [14]–[18], they typically require annotated datasets and greater computational resources. In contrast, K-means clustering provides an efficient and unsupervised alternative suitable for deployment in low-resource or real-time systems.

The experimental results have important implications for the practical deployment of ultrasound tomography in clinical and low-cost diagnostic settings. In particular, the method's robustness in under-sampled conditions (*i.e.*, when the number of measurements is fewer than the number of variables) suggests its suitability for real-world scenarios where sensor access or scan duration is limited. The combined use of median filtering and K-means clustering offers a compact and explainable enhancement pipeline that can be

integrated into point-of-care ultrasound systems. Moreover, this framework can improve diagnostic accuracy by preserving object integrity and suppressing spurious artifacts, especially in applications such as breast cancer screening in young women where ultrasound outperforms mammography.

Despite the promising results, there are several limitations to our current approach. First, all experiments were conducted on synthetic datasets generated using simulated scattering models. Although we introduced additive Gaussian noise to emulate real-world imperfections, the generalizability of the proposed method to real clinical data remains to be tested. Second, the use of a fixed-size median filter may not adapt optimally to different noise distributions or object geometries. Third, while K-means clustering is computationally lightweight, it assumes the number of regions is known a priori and may not handle complex or heterogeneous tissue structures effectively.

Machine learning may use all data and information what it has already, beside that machine learning can produce result this more accurate than older result. Machine learning not only make automation is growing up but also decreasing the possibility that the human operator will make some errors. Over past few year, various machine learning techniques have been utilized to enhance the reliability of ultrasound-nondestructive testing [23]–[28]. Future work will focus on validating the proposed approach on experimental and clinical ultrasound data to assess its real-world applicability. We also plan to explore adaptive filtering techniques, such as anisotropic diffusion or guided filters, that can adjust based on local image characteristics. Furthermore, the segmentation step can be improved by integrating region-growing or active contour methods to better handle irregularly shaped lesions. Finally, hybrid frameworks combining the current physics-based inversion with learning-based priors or data-driven regularizers may yield further improvements in reconstruction quality, especially in challenging imaging scenarios.

5. CONCLUSION

In this work, we propose and evaluate the implementation of a median filter as a means to address the noise artifacts that commonly afflict reconstructed images obtained through the DBIM. Initial findings indicate a noteworthy decrease in noise levels within the reconstructed images, thereby fostering a heightened degree of diagnostic clarity. The median filter adeptly retains crucial anatomical intricacies while simultaneously mitigating undesirable noise artifacts, thereby culminating in an overarching enhancement of the quality of ultrasound tomographic reconstructions. Additionally, the incorporation of a rudimentary machine learning algorithm, specifically K-means clustering, facilitates the automatic segmentation of the reconstructed image into distinct partitions, delineating objects, background, and noise regions with precision. The outcomes underscore the efficacy of K-means clustering in accurately demarcating regions within images generated via the filtered DBIM approach, with a prominent observation being the marked reduction in noise evident in the images reconstructed utilizing this method. Consequently, these combined methodologies not only serve to ameliorate the visual fidelity of ultrasound tomographic reconstructions but also contribute to streamlining the diagnostic interpretation process through the elucidation of clear and well-defined image components.

REFERENCES

[1] R. Highnam, M. Brady, and B. Shepstone, "A representation for mammographic image processing," *Medical Image Analysis*, vol. 1, no. 1, pp. 1–18, Mar. 1996, doi: 10.1016/s1361-8415(01)80002-5.

[2] E. D. Pisano and M. J. Yaffe, "Digital mammography," *Radiology*, vol. 234, no. 2, pp. 353–362, Feb. 2005, doi: 10.1148/radiol.2342030897.

[3] E. L. Madsen, J. A. Zagzebski, G. R. Frank, J. F. Greenleaf, and P. L. Carson, "Anthropomorphic breast phantoms for assessing ultrasonic imaging system performance and for training ultrasonographers: Part II," *Journal of Clinical Ultrasound*, vol. 10, no. 3, pp. 91–100, 1982, doi: 10.1002/jcu.1870100302.

[4] T. L. Szabo, "Therapeutic ultrasound," in *Diagnostic Ultrasound Imaging: Inside Out*, Elsevier, 2014, pp. 735–763, doi: 10.1016/b978-0-12-396487-8.00017-3.

[5] A. Seibert and J. Boone, "X-ray imaging physics for nuclear medicine technologists. Part 2: X-ray interactions and image formation," *Journal of Nuclear Medicine Technology*, vol. 33, no. 1, pp. 3–18, 2005.

[6] I. Cunningham and P. Judy, "Computed tomography," in *The Biomedical Engineering Handbook, Second Edition. 2 Volume Set*, CRC Press, 1999, doi: 10.1201/9781420049510.ch62.

[7] M. T. Vlaardingerbroek and J. A. den Boer, *Magnetic resonance imaging: Theory and practice*. Springer Berlin Heidelberg, 1996, doi: 10.1007/978-3-662-03258-9.

[8] W. C. Chew and Y. M. Wang, "Reconstruction of two-dimensional permittivity distribution using the distorted Born iterative method," *IEEE Transactions on Medical Imaging*, vol. 9, no. 2, pp. 218–225, Jun. 1990, doi: 10.1109/42.56334.

[9] M. L. Tracy and S. A. Johnson, "Inverse scattering solutions by a sinc basis, multiple source, moment method – Part II: Numerical evaluations," *Ultrasonic Imaging*, vol. 5, no. 4, pp. 376–392, Oct. 1983, doi: 10.1177/016173468300500407.

[10] O. S. Haddadin, S. D. Lucas, and E. S. Ebbini, "Solution to the inverse scattering problem using a modified distorted Born iterative algorithm," in *1995 IEEE Ultrasonics Symposium. Proceedings. An International Symposium*, vol. 2, 1995, pp. 1411–1414, doi: 10.1109/ultsym.1995.495819.

[11] J. F. Greenleaf, J. Ylitalo, and J. J. Gisvold, "Ultrasonic computed tomography for breast examination," *IEEE Engineering in Medicine and Biology Magazine*, vol. 6, no. 4, pp. 27–32, Dec. 1987, doi: 10.1109/memb.1987.5006465.

[12] M. P. André, H. S. Janée, P. J. Martin, G. P. Otto, B. A. Spivey, and D. A. Palmer, "High-speed data acquisition in a diffraction tomography system employing large-scale toroidal arrays," *International Journal of Imaging Systems and Technology*, vol. 8, no. 1, pp. 137–147, 1997, doi: 10.1002/(SICI)1098-1098(1997)8:1<137::AID-IMA15>3.3.CO;2-1.
[13] J. Wiskin, D. T. Borup, S. A. Johnson, M. Berggren, T. Abbott, and R. Hanover, "Full-wave, non-linear, inverse scattering: High resolution quantitative breast tissue tomography," in *Acoustical Imaging*, Springer Netherlands, 2007, pp. 183–193, doi: 10.1007/1-4020-5721-0_20.
[14] H. You and G. Rumbe, "Comparative study of classification techniques on breast cancer FNA biopsy data," *International Journal of Interactive Multimedia and Artificial Intelligence*, vol. 1, no. 3, p. 5, 2010, doi: 10.9781/ijimai.2010.131.
[15] S.-H. Chen, C.-W. Wang, I.-H. Tai, K.-P. Weng, Y.-H. Chen, and K.-S. Hsieh, "Modified YOLOv4-DenseNet algorithm for detection of ventricular septal defects in ultrasound images," *International Journal of Interactive Multimedia and Artificial Intelligence*, vol. 6, no. 7, p. 101, 2021, doi: 10.9781/ijimai.2021.06.001.
[16] M. Micucci and A. Iula, "Recent advances in machine learning applied to ultrasound imaging," *Electronics*, vol. 11, no. 11, p. 1800, Jun. 2022, doi: 10.3390/electronics11111800.
[17] L. Pehrson, C. Lauridsen, and M. Nielsen, "Machine learning and deep learning applied in ultrasound," *Ultraschall in der Medizin - European Journal of Ultrasound*, vol. 39, no. 04, pp. 379–381, Aug. 2018, doi: 10.1055/a-0642-9545.
[18] A. K. Mishra, P. Roy, S. Bandyopadhyay, and S. K. Das, "Breast ultrasound tumour classification: a machine learning—Radiomics based approach," *Expert Systems*, vol. 38, no. 7, May 2021, doi: 10.1111/exsy.12713.
[19] R. Lavarello and M. Oelze, "A study on the reconstruction of moderate contrast targets using the distorted born iterative method," *IEEE Transactions on Ultrasonics, Ferroelectrics and Frequency Control*, vol. 55, no. 1, pp. 112–124, 2008, doi: 10.1109/tuffc.2008.621.
[20] Q.-H. Tran, D.-T. Tran, H. T. Huynh, L. Ton-That, and L.-T. Nguyen, "Influence of dual-frequency combination on the quality improvement of ultrasound tomography," *SIMULATION: Transactions of The Society for Modeling and Simulation International*, vol. 92, no. 3, pp. 267–276, Feb. 2016, doi: 10.1177/0037549716630605.
[21] A. V. Goncharsky, S. Yu. Romanov and S. Yu. Seryozhnikov, "Low-frequency 3D ultrasound tomography: dual-frequency method," *Numerical Methods and Programming (Vychislitel'nye Metody i Programmirovanie)*, vol. 19, no. 4, pp. 479–495, Dec. 2018, doi: 10.26089/nummet.v19r443.
[22] T. Q. Huy, V. D. Nguyen, C. T. P. Dung, B. T. Ninh, and T. D. Tan, "An efficient procedure of multi-frequency use for image reconstruction in ultrasound tomography," in *Intelligent Computing in Engineering*, Springer Singapore, 2020, pp. 921–929, doi: 10.1007/978-981-15-2780-7_97.
[23] R. J. Pyle, R. L. T. Bevan, R. R. Hughes, R. K. Rachev, A. A. S. Ali, and P. D. Wilcox, "Deep learning for ultrasonic crack characterization in NDE," *IEEE Transactions on Ultrasonics, Ferroelectrics, and Frequency Control*, vol. 68, no. 5, pp. 1854–1865, May 2021, doi: 10.1109/tuffc.2020.3045847.
[24] T. Li, "From zero crossings to quantile-frequency analysis of time series with an application to nondestructive evaluation," *Applied Stochastic Models in Business and Industry*, vol. 36, no. 6, pp. 1111–1130, Dec. 2019, doi: 10.1002/asmb.2499.
[25] V. Nasir, H. Fathi, and S. Kazemirad, "Combined machine learning–wave propagation approach for monitoring timber mechanical properties under UV aging," *Structural Health Monitoring*, vol. 20, no. 4, pp. 2035–2053, 2021, doi: 10.1177/1475921721995987.
[26] M. Soltani Firouz, A. Farahmandi, and S. Hosseinpour, "Early detection of freeze damage in navel orange fruit using nondestructive low intensity ultrasound coupled with machine learning," *Food Analytical Methods*, vol. 14, no. 6, pp. 1140–1149, Jan. 2021, doi: 10.1007/s12161-020-01942-w.
[27] M. A. Oliveira, E. F. Simas Filho, M. C. S. Albuquerque, Y. T. B. Santos, I. C. da Silva, and C. T. T. Farias, "Ultrasound-based identification of damage in wind turbine blades using novelty detection," *Ultrasonics*, vol. 108, p. 106166, Dec. 2020, doi: 10.1016/j.ultras.2020.106166.
[28] L. C. Silva, E. F. Simas Filho, M. C. S. Albuquerque, I. C. Silva, and C. T. T. Farias, "Embedded decision support system for ultrasound nondestructive evaluation based on extreme learning machines," *Computers & Electrical Engineering*, vol. 90, p. 106891, Mar. 2021, doi: 10.1016/j.compeleceng.2020.106891.

BIOGRAPHIES OF AUTHORS

Nguyen Quang Huy received the bachelor of science with upper second class honors in computer science and information systems at Oxford Brookes University in 2014 and master degree on information and communication technology at University of Science and Technology of Hanoi and National Polytechnic Institute of Toulouse (France) in 2017. Now, he is researcher and he is working at the Institute of Information Technology, Vietnam Academy of Science and Technology. His researches focus on artificial intelligence, data mining, soft computing, and fuzzy computing. He can be contacted at email: quanghuy7889@gmail.com.

Nguyen Truong Thang received a Ph.D. in 2005 at the Japan Advanced Institute of Science and Technology (JAIST), Japan. Currently, he is working at the Institute of Information Technology, Vietnam Academy of Science and Technology. His major research fields include software quality assurance, software verification, program analysis, data mining and machine learning. He can be contacted at email: ntthang@ioit.ac.vn.